JOURNAL OF THERMOPHYSICS AND HEAT TRANSFER
Vol. 18, No. 4, October–December 2004

Mixed Convection Cooling of Heat Sources Mounted with Porous Blocks

P. C. Huang,* C. F. Yang,† and S. Y. Chang†
National Taipei University of Technology, Taipei 106, Taiwan, Republic of China

A numerical study is performed to analyze laminar mixed convection in a parallel-plate vertical channel with discrete strip heat sources on one channel wall. The effect on heat transfer of a porous block mounted above each heat source is considered. The Brinkman–Forchheimer–Extended Darcy model with the Boussinesq approximation is used to characterize the flowfield inside the porous region. Solution of the coupled governing equations for the porous/fluid composite system is obtained by utilizing a control volume method through the use of a stream function–vorticity approach. The characteristics of fluid flow and mixed convection heat transfer have been obtained by the examination of various governing parameters such as the Darcy number, Reynolds number, inertia parameter, Grashof number, conductivity ratio, and geometric parameter. The results indicate that the size and strength of recirculating flow induced by the porous block make significant changes in the cooling of strip heater, especially at both trailing and leading edges of heaters. In addition, it is shown that specific choices in porous block shape, permeability, and thermal conductivity can produce profound effects on the flow and heat transfer characteristics.

Nomenclature

Da	=	Darcy number, K/R^2
F	=	function used in expressing inertia terms
Gr_f	=	Grashof number, $g\beta q'' R^4/k_f \nu_f^2$
Gr_{eff}	=	modified Grashof number, $g\beta q'' K R^2/k_{\text{eff}} \nu_{\text{eff}}^2$
g	=	gravitational acceleration, m^2/s
H	=	height of porous block, m
h	=	convective heat transfer coefficient, W/m$^2 \cdot$ K
K	=	permeability of the porous medium, m^2
k	=	thermal conductivity, W/m K
L	=	length of the channel, as shown in Fig. 1, m
L_i	=	length of plate upstream from the heat-source array, m
L_o	=	length of plate downstream from the heat-source array, m
Nu	=	Nusselt number, hx/k_f
Nu_m	=	average Nusselt number over one heat source
P	=	pressure, Pa
P_i	=	pressure at channel inlet, Pa
Pe	=	Peclet number, $u_{\text{av}} R/\alpha$
Pr	=	Prandtl number, ν/α
q''	=	uniform heat flux from each heat source, W/m^2
R	=	height of channel, m
Re	=	Reynolds number, $u_{\text{av}} R/\nu$
S	=	spacing between heat sources or porous blocks
T	=	temperature, K
T_i	=	uniform inlet temperature, K
u	=	x-component velocity, m/s
$\boldsymbol{V}$	=	velocity vector, m/s
v	=	y-component velocity, m/s
W	=	width of heat source or porous block, m
x	=	horizontal coordinate, m
y	=	vertical coordinate, m
α	=	thermal diffusivity, m^2/s
α_{eff}	=	effective thermal diffusivity, $k_{\text{eff}}/\rho_f c_{p,f}$, m^2/s
β	=	thermal expansion coefficient of fluid, K^{-1}
ε	=	porosity of the porous medium
Λ	=	inertial parameter, $FL\epsilon/\sqrt{K}$
λ	=	thermal conductivity ratio, k_{eff}/k_f
μ	=	dynamic viscosity, kg/m $\cdot$ s
ν	=	kinematic viscosity, m^2/s
ξ	=	vorticity
φ	=	stream function

Subscripts

av	=	average
eff	=	effective
f	=	fluid
I	=	interface
i	=	inlet
P	=	porous
x	=	local
w	=	wall
o	=	outlet

Superscript

*	=	dimensionless quantity

Introduction

THERMAL control of electronic equipment and devices has received considerable attention by investigators in the past few decades. A primary requirement in the thermal control of the electronic components is to maintain the temperature of the electronic component equal to or below a maximum operation temperature. For reliable operation, different high-effective cooling techniques[1] have been used to obtain a well-controlled thermal environment, including the traditional methods of natural and forced convective cooling. One of the promising techniques is the application of a porous material due to its large fluid contact surface area per unit volume and the enhanced flow mixing caused by the tortuous path of the porous matrix in the thermal dispersion process.

Thermal convection in fluid-saturated porous media has been of continuing interest because of its relevance in a broad range of engineering applications such as thermal insulation, heat exchanger, geothermal energy systems, enhanced oil recovery, heat pipe technology, industrial furnace, cooling of electronic equipment, etc. A comprehensive review of the existing studies on these topics can be found in Ref. 2.

Received 21 October 2003; revision received 13 March 2004; accepted for publication 19 April 2004.

*Assistant Professor, Department of Air-Conditioning and Refrigerating Engineering, 1, Section 3, Chung-Hsiao East Road; pchuang@ntut.edu.tw.
†Graduate Student, Department of Air-Conditioning and Refrigerating Engineering.

For the problem of mixed convection in a vertical channel or annuli fully packed with a porous material, Koh and Colony[3] modeled the microstructures of integrated circuits as a vertical channel filled with porous media to investigate the heat transfer by using Darcy's law. Tien and Kuo[4] simulated the same cooling system based on the modified Darcy's equation to demonstrate the significance of no-slip boundary conditions. Kuo and Lu[5] solved fully developed laminar mixed convection problems with different kinds of thermal boundary conditions. Hadim[6] reported on mixed convection in a vertical porous channel maintained at uniform wall temperature to explore the evolution of mixed convection in the entrance region using a Brinkman–Forchheimer–extended Darcy model. Numerical and experimental studies of mixed convection in vertical porous annuli were conducted by Reda[7] and Choi et al.[8]

Among these studies, the heat transfer of a vertical fully/partially porous channel with discrete heat sources was of special interest because of its applications for the cooling of electronics. Lai et al.[9] numerically analyzed mixed convection in a vertical porous layer with a finite wall heat source using Darcy's law. They found that a recirculatory secondary flow exists in the channel. For a favorable flow, the heat transfer rate increases monotonically with the increasing velocity, and for the opposing flow with increasing Peclet number, the heat transfer rate first decreases and reaches a minimum before starting to increase again. Hadim and Chen[10] solved the problem of buoyancy-assisted mixed convection in a vertical porous channel with discrete heat sources on one wall. Their results indicate that, as the Darcy number is decreased, the location of flow separation from the cold wall did not change, whereas reattachment moved farther downstream. The heat transfer rate increased with decreasing Darcy number, and the effect of Darcy number is more pronounced over the first heat source. Most of these studies are related to the aspect of mixed convection over the full porous system, however, the problem of combining forced and free convection in a fluid/porous composite system and the different thermal properties among the composite systems has been discussed to some extent.

This paper presents a numerical study of mixed convection in a parallel-plate vertical channel with discrete heat sources flush mounted on a wall. The porous block attached over each heat source is considered as an effective heat sink for thermal management of electronic devices. In this work, the basic interaction phenomena between the porous substrate and the fluid region for these fluid/porous composite systems as well as the methodology for enhancing the heat transfer rate along the heat source have been analyzed. Furthermore, the influences of various parameters governing the hydrodynamic and thermal characteristics of the problem are examined to establish the fundamental effects and provide practical results. It is shown that specific choices of descriptive parameters can exert a significant influence on the flow and thermal characteristics. For example, choosing a particular porous block shape in combination with an appropriate thermal conduction and permeability can improve heat transfer in a local region.

Mathematical Formulation

The configuration for the problem under investigation is shown in Fig. 1a. It includes the flow through a vertical parallel-plate channel with discrete heat sources on the right plate. The channel has a height R and length L. The heat sources of equal length are placed at equal interval S, and the first one is located at a distance L_i from the channel entrance. Every heat source dissipates an equal and uniform heat flux q'' over its length W. The porous block, with height H and width W, mounted on each heat source is used as heat sink. The flow is assumed to be steady, incompressible, and two dimensional. The porous medium is completely saturated with the fluid and is considered to be isotropic, homogeneous, and in local thermal equilibrium. The thermophysical properties of both the fluid and the porous medium are assumed constant except for the fluid density in the buoyancy term of the momentum equation. Possible channeling near the wall is neglected in the present study because fibrous media are considered for which the porosity and permeability are relatively constant even close to the wall.[11] Radiation has also been neglected, and therefore, the study results are applicable for moderate temperature differences. In this work, the flow is modeled by the Darcy–Brinkman–Forchheimer equation in the porous matrix to incorporate the viscous and inertial effects (see Ref. 12), by Navier–Stokes equation in the fluid domain, and by the energy equation in the thermal field. Based on the Boussinesq approximation and constant thermal dispersion (incorporated in the effective thermal conductivity), an efficient alternative method combining the two sets of conservation equations for the fluid and porous regions into one set of conservation equations is to model the porous substrate and the flow regions as a single domain governed by one set of conservation equations, the solution of which satisfies the matching conditions at the fluid/porous interfaces. The mentioned resulting momentum and energy equations in terms of dimensionless variables are[10,13]

$$\frac{\partial\varphi^*}{\partial y^*}\frac{\partial\xi^*}{\partial x^*}-\frac{\partial\varphi^*}{\partial x^*}\frac{\partial\xi^*}{\partial y^*}=\frac{1}{Re}\nabla^2\xi^*-\frac{Gr}{Re^2}\frac{\partial T^*}{\partial y^*}+S_\varphi \tag{1}$$

$$\nabla^2\varphi^*=-\xi^* \tag{2}$$

$$\frac{\partial\varphi^*}{\partial y^*}\frac{\partial T^*}{\partial x^*}-\frac{\partial\varphi^*}{\partial x^*}\frac{\partial T^*}{\partial y^*}=\nabla\cdot\left(\frac{1}{Pe}\nabla T^*\right) \tag{3}$$

where x^* and y^* are dimensionless rectangular Cartesian coordinates and φ and ξ are the stream function and vorticity, respectively, which are related to the fluid velocity components u and v by

$$u=\frac{\partial\varphi}{\partial y},\qquad v=-\frac{\partial\varphi}{\partial x},\qquad \xi=\frac{\partial v}{\partial x}-\frac{\partial u}{\partial y} \tag{4}$$

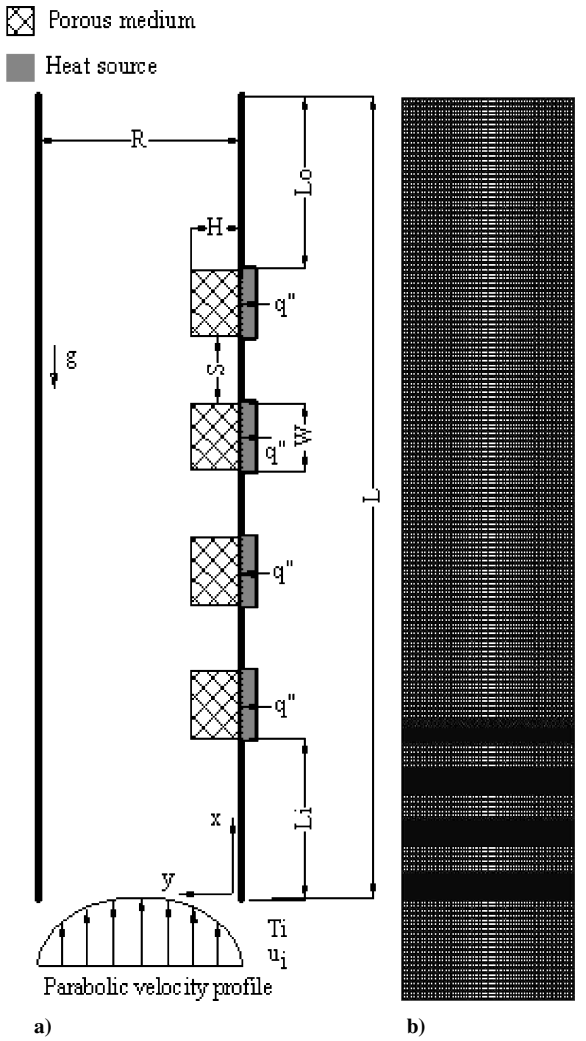

Fig. 1 Present configuration: a) schematic diagram and corresponding coordinate systems and b) typical nonuniform grid system for the whole computational domain.

The nondimensional parameters in the fluid region are

$$Re_f = u_{\text{av}} R/\nu_f, \qquad Pe_f = u_{\text{av}} R/\alpha_f$$

$$Gr_f = g\beta q'' R^4 \Big/ k_f \nu_f^2, \qquad S_\varphi = 0 \tag{5}$$

and in the porous region the nondimensional parameters are

$$Re_{\text{eff}} = \frac{u_{\text{av}} R}{\nu_{\text{eff}}}, \qquad Pe_{\text{eff}} = \frac{u_{\text{av}} R}{\alpha_{\text{eff}}}, \qquad Gr_{\text{eff}} = \frac{g\beta q'' K R^2}{k_{\text{eff}} \nu_{\text{eff}}^2}$$

$$Da = \frac{K}{R^2}, \qquad \Lambda = \frac{FR\varepsilon}{\sqrt{K}} \tag{6}$$

$$S_\varphi = -\frac{1}{Re_{\text{eff}} Da}\xi^* - \Lambda|\bar{V}^*|\xi - \Lambda\left[v^* \frac{\partial|\bar{V}^*|}{\partial x^*} - u^* \frac{\partial|\bar{V}^*|}{\partial y^*}\right] \tag{7}$$

The source term S_φ can be considered as those contributing to the vorticity generation due to the presence of the rectangular porous blocks. Note that modified Grashof number Gr_{eff}, Grashof number Gr_f, and Darcy number Da are related by $Gr_{\text{eff}} = Gr_f Da/\lambda$, where $\lambda = k_{\text{eff}}/k_{\text{f}}$, and k_{eff} is the effective conductivity of porous medium and k_{f} is that of the fluid. All of the preceding variables have been nondimensionalized based on the following definitions:

$$x^* = x/R, \qquad y^* = y/R, \qquad L_i^* = L_i/R, \qquad L_o^* = L_o/L$$

$$L^* = L/R, \qquad u^* = u/u_{\text{av}}, \qquad v^* = v/u_{\text{av}} \tag{8a}$$

$$H^* = H/R, \qquad W^* = W/R, \qquad S^* = S/R$$

$$|\bar{V}^*| = \sqrt{u^{*2} + v^{*2}}, \qquad \varphi^* = \varphi/u_{\text{av}} R, \qquad \xi^* = R\xi/u_{\text{av}} \tag{8b}$$

$$T^* = (T - T_i)/(q'' R/k_f), \qquad Pr = \nu/\alpha, \qquad P^* = P \Big/ \rho u_{\text{av}}^2 \tag{8c}$$

where

$$u_{\text{av}} = \left(\int_0^A u \, \mathrm{d}A\right) \Big/ A$$

A is the cross section area of the channel. Noted that these conservation equations for mixed convection in the porous region are developed here using the local volume-averaging technique.[12]

The boundary conditions for the configuration shown in Fig. 1a are such that the no-slip condition occurs at the two impermeable walls. At the channel inlet, the fluid has an upward fully developed, parabolic velocity profile of uniform temperature distribution T_i. At the right wall, there is a uniform heat flux q'', which is distributed over each heat source, and the portion of the wall between heat sources is adiabatic. The left wall is entirely adiabatic. At the channel exit, the boundary condition was determined by the fully developed condition. At the porous/fluid interface, the following quantities evaluated in both the porous and fluid regions are matched: horizontal and vertical velocities, normal and shear stresses, temperature, pressure, and heat flux. In summary, the boundary conditions can be described in the following dimensionless form:

1) At the inlet, $x^* = 0$ and $0 < y^* < 1$,

$$u^* = 6y^*(1 - y^*), \qquad v^* = 0, \qquad T^* = 0$$

$$\varphi^* = 6\left(y^{*2}\Big/2 - y^{*3}\Big/3\right), \qquad \xi^* = -6(1 - 2y^*) \tag{9}$$

2) At the outlet, $x^* = L^*$ and $0 \le y^* \le 1$,

$$\frac{\partial T^*}{\partial y^*} = 0, \qquad \frac{\partial \varphi^*}{\partial x^*} = 0, \qquad \frac{\partial \xi^*}{\partial x^*} = 0 \tag{10}$$

3) At the left channel wall, $0 \leqq x^* \leqq L^*$ and $y^* = 1$,

$$u^* = 0, \qquad v^* = 0, \qquad \varphi^* = 1$$

$$\xi^* = -\frac{\partial^2 \varphi^*}{\partial y^{*2}}, \qquad \frac{\partial T^*}{\partial y^*} = 0 \tag{11}$$

4) At the right channel wall, $0 \leqq x^* \leqq L^*$ and $y^* = 0$,

$$u^* = 0, \qquad v^* = 0, \qquad \varphi^* = 0, \qquad \xi^* = -\frac{\partial^2 \varphi^*}{\partial y^{*2}}$$

$$\frac{\partial T^*}{\partial y^*} = \begin{cases} 0 & \text{(at insulated area)} \\ -1 & \text{(at heat source area)} \end{cases} \tag{12}$$

5) Along the porous/fluid interface,

$$u_p^*\big|_{g(x,y)=0} = u_f^*\big|_{g(x,y)=0}, \qquad v_p^*\big|_{g(x,y)=0} = v_f^*\big|_{g(x,y)=0}$$

$$\mu_{\text{eff}} \frac{\partial v_p^*}{\partial n^*}\bigg|_{g(x,y)=0} = \mu_f \frac{\partial v_f^*}{\partial n^*}\bigg|_{g(x,y)=0} \tag{13a}$$

$$\mu_{\text{eff}}\left[\frac{\partial u_p^*}{\partial n^*} + \frac{\partial v_p^*}{\partial t^*}\right]\bigg|_{g(x,y)=0} = \mu_f\left[\frac{\partial u_f^*}{\partial n^*} + \frac{\partial v_f^*}{\partial t^*}\right]\bigg|_{g(x,y)=0} \tag{13b}$$

$$T_P^*\big|_{g(x,y)=0} = T_f^*\big|_{g(x,y)=0}, \qquad k_{\text{eff}} \frac{\partial T_P^*}{\partial n^*}\bigg|_{g(x,y)=0} = k_f \frac{\partial T_f^*}{\partial n^*}\bigg|_{g(x,y)=0} \tag{13c}$$

where $g(x, y) = 0$ are the curves defining the porous/fluid interfaces and the derivative with respect to n and t represents the normal and tangential gradients, respectively, to these curves at any point on the interfaces.

For further insight into the effects of porous material on the heat transfer rate at the heat source, the local Nusselt number is defined as

$$Nu_x = \frac{hR}{k_f} = \frac{q''R}{(T_w - T_i)k_f} \tag{14}$$

The average Nusselt number over one heat source is evaluated as follows:

$$Nu_m = \int_{W_i} Nu_x \, \mathrm{d}x \Big/ W \tag{15}$$

Note that the definition of Nusselt number based on the conductivity of the fluid permits a direct comparison for a heat source with and without porous block.

Numerical Method

With use of a nonuniform rectangular grid system, the finite difference form of the vorticity transport, stream function, and energy equations were derived using control volume integration of these differential equations over discrete cells surrounding the grid points. Figure 1b shows a typical nonuniform grid system employed for the present calculations. This grid system was designed to capture the steep gradients near the walls, the porous/fluid interfaces, and the porous block. In the described discretization scheme, the second-order upwind and central-differencing formats are introduced for the convective and diffusive terms, respectively. The finite difference equations thus obtained were solved by the extrapolated-Jacobi scheme. This iterative scheme is based on a double-cyclic routine, which translates into a sweep of only half of the grid points at each iteration step.[14] In this study, convergence was considered to have been achieved when the absolute value of relative error on each grid point between two successive iterations was found to be less than 10^{-6}.

The interface between the porous medium and fluid space requires special consideration. This is due to the sharp change of the thermophysical properties, such as the permeability, porosity, and the thermal conductivity, across the interface. All of these effects on the porous/fluid interface are summarized in the dimensional parameters Reynolds number Re, Grashof number Gr, Darcy number Da, Λ, and Prandtl number Pr. The harmonic mean formulation suggested by Patankar[15] was used to handle these discontinuous

characteristics in the porous/fluid interface. For the present case, Reynolds number Re, Grashof number Gr, Darcy number Da, Λ, and Prandtl number Pr at the interface of a control volume are as follows:

$$Re_I = \frac{2Re_{\text{eff}}Re_f}{Re_{\text{eff}} + Re_f}, \qquad Da_I = \frac{2Da_{\text{eff}}Da_f}{Da_{\text{eff}} + Da_f}$$

$$Gr_I = \frac{2Gr_{\text{eff}}Gr_f}{Gr_{\text{eff}} + Gr_f}, \qquad \Lambda_I = \frac{2\Lambda_{\text{eff}}\Lambda_f}{\Lambda_{\text{eff}} + \Lambda_f}$$

$$Pr_I = \frac{2Pr_{\text{eff}}Pr_f}{Pr_{\text{eff}} + Pr_f} \tag{16}$$

Therefore, instead of the source terms in Eqs. (5) and (7), the following source terms were used across the interface:

$$S_\varphi = \frac{u^*}{Re_I}\frac{\partial}{\partial y^*}\left(\frac{1}{Da_I}\right) - \frac{v^*}{Re_I}\frac{\partial}{\partial x^*}\left(\frac{1}{Da_I}\right) + |\bar{V}^*|u^*\frac{\partial}{\partial y^*}(\Lambda_I) - |\bar{V}^*|v^*\frac{\partial}{\partial x^*}(\Lambda_I) - T^*\left[\frac{1}{Re_I^2}\frac{\partial}{\partial y^*}(Gr_I) - Gr_I\frac{\partial}{\partial y^*}\left(\frac{1}{Re_I^2}\right)\right] \tag{17}$$

$$S_\varphi = -\frac{1}{Re_I Da_I}\xi^* - \Lambda_I|\bar{V}^*|\xi^* - \Lambda_I\left[v^*\frac{\partial|\bar{V}^*|}{\partial x^*} - u^*\frac{\partial|\bar{V}^*|}{\partial y^*}\right] + \frac{u^*}{Re_I}\frac{\partial}{\partial y^*}\left(\frac{1}{Da_I}\right) - \frac{v^*}{Re_I}\frac{\partial}{\partial x^*}\left(\frac{1}{Da_I}\right) + |\bar{V}^*|u^*\frac{\partial}{\partial y^*}(\Lambda_I) - |\bar{V}^*|v^*\frac{\partial}{\partial x^*}(\Lambda_I) - T^*\left[\frac{1}{Re_I^2}\frac{\partial}{\partial y^*}(Gr_I) - Gr_I\frac{\partial}{\partial y^*}\left(\frac{1}{Re_I^2}\right)\right] \tag{18}$$

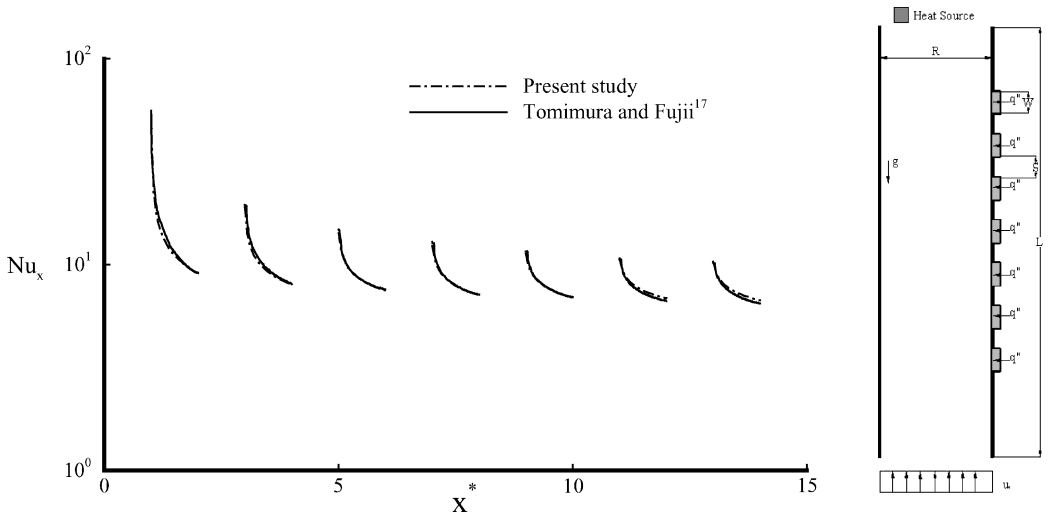

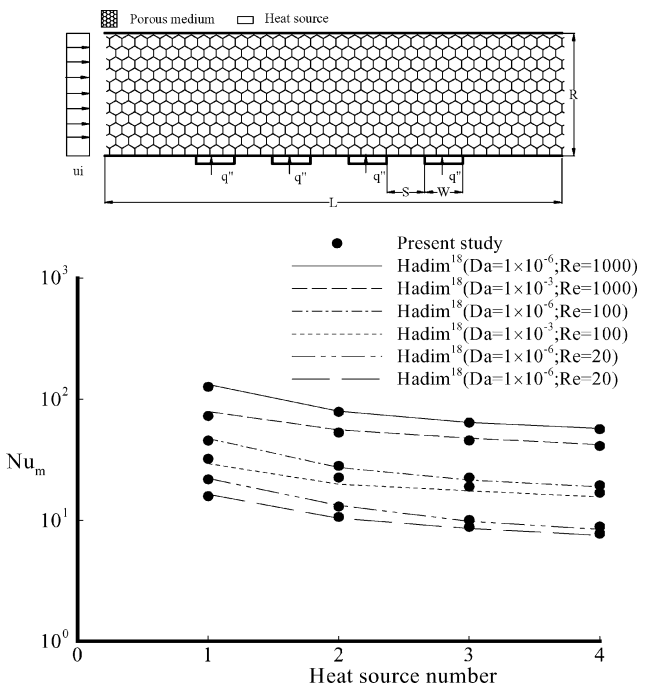

Fig. 2 Nusselt number comparisons: a) local Nusselt number distribution in nonporous channel containing seven heat sources vs solution given by Tomimura and Fujii[17] for $S^* = 1$, $W^* = 1$, $L^* = 15$, $Pr = 0.7$, $Re = 500$, and $Gr_f = 1 \times 10^6$, and b) average Nusselt number over each heat source vs that Hadim[18] result for flow in full porous channel with $\Lambda = 0.1$, $S^* = 1$, $W^* = 1$, $Pr = 10$, and $k_{\text{eff}}/k_f = 1$ at $Da = 1 \times 10^{-6}$ and 1×10^{-3} for $Re = 20$, 100, and 1000.

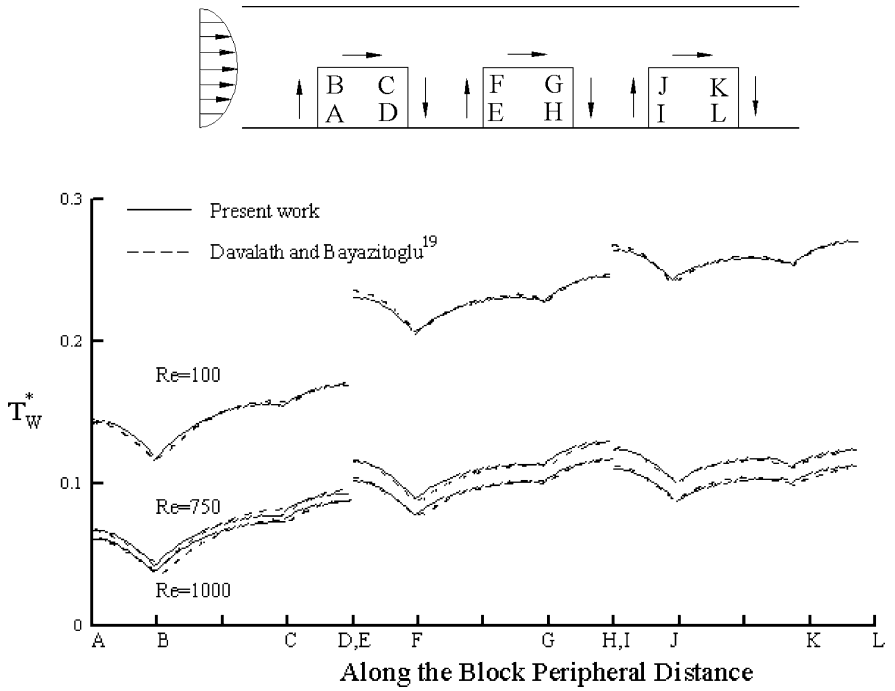

Fig. 3 Comparison of dimensionless wall temperature distribution along exposed faces of three heated blocks with the solution given by Davalath and Bayazitoglu[19] for $S^* = 0.5$, $W^* = 0.5$, $H^* = 0.25$, $L_i^* = 3.0$, $L_o^* = 9.5$, $Pr = 0.7$, and $k_s/k_f = 10$ at $Re = 100$, 750, and 1000.

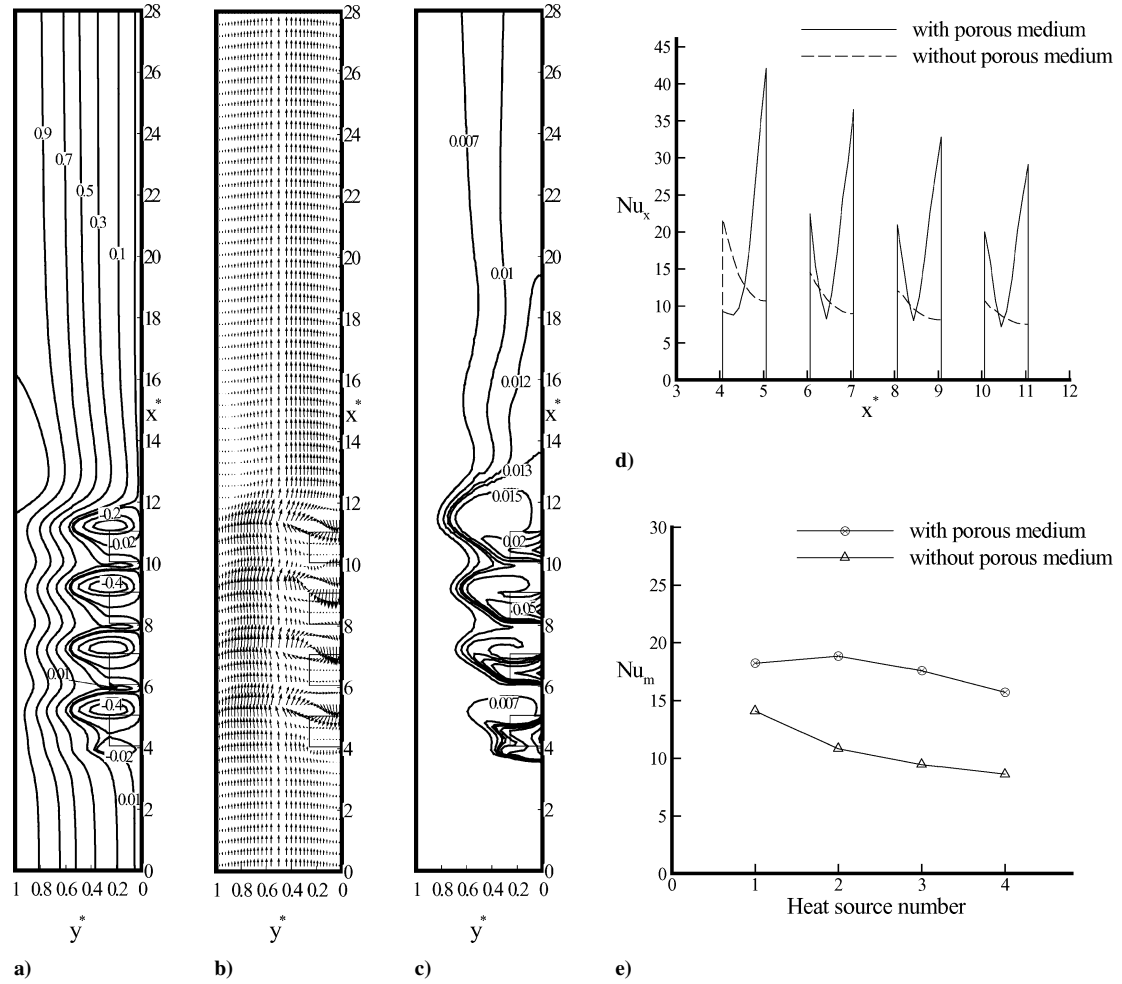

Fig. 4 Flow in vertical parallel-plate channel containing multiple porous-covering heat sources on right plate for $Da = 1 \times 10^{-5}$, $\Lambda = 0.35$, $Re = 600$, $Gr_f = 3.6 \times 10^5$, $Pr = 0.7$, $\lambda = 1$, $H^* = 0.25$, $W^* = 1.0$, $S^* = 1.0$, $L_i^* = 4$, and $L_o^* = 28$: a) streamlines, b) velocity distribution, c) isotherms, d) local Nusselt number distribution, and e) average Nusselt number.

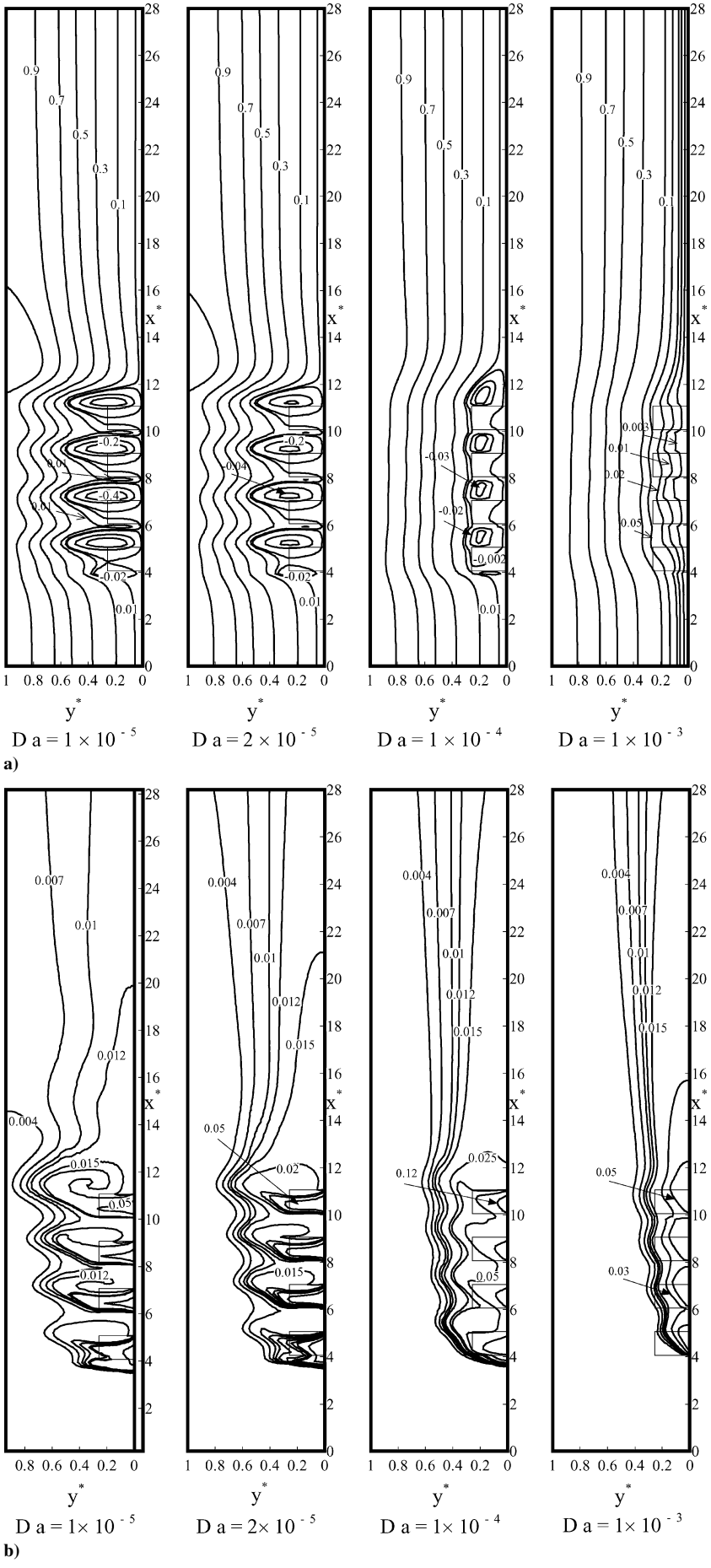

Fig. 5 Effects of the Darcy number for $Re = 600$, $\Lambda = 0.35$, $Pr = 0.7$, $Gr_f = 3.6 \times 10^5$, $\lambda = 1$, $H^* = 0.25$, $W^* = 1.0$, $S^* = 1.0$, $L_i^* = 4$, and $L_o^* = 28$ on a) streamlines, b) isotherms, c) local Nusselt number distributions, and d) average Nusselt number.

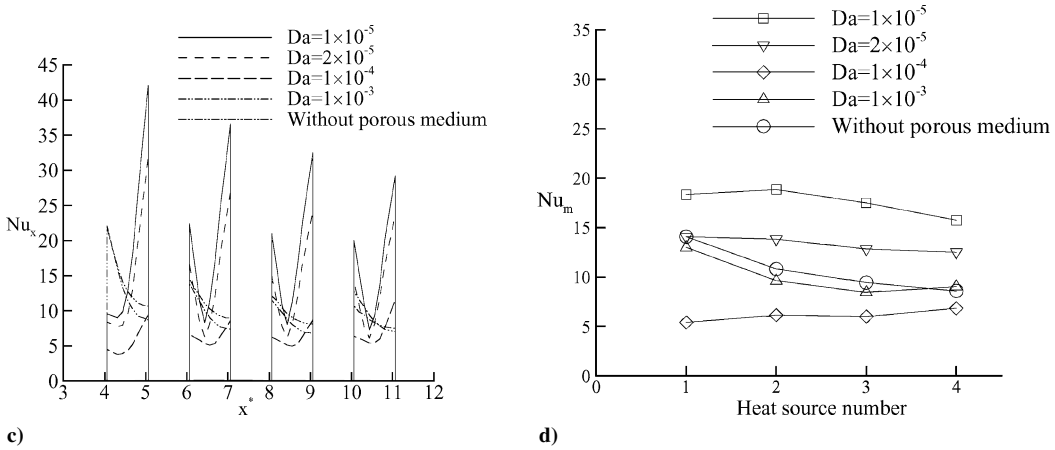

Fig. 5 Effects of the Darcy number for $Re = 600$, $\Lambda = 0.35$, $Pr = 0.7$, $Gr_f = 3.6 \times 10^5$, $\lambda = 1$, $H^* = 0.25$, $W^* = 1.0$, $S^* = 1.0$, $L_i^* = 4$, and $L_o^* = 28$ on a) streamlines, b) isotherms, c) local Nusselt number distributions, and d) average Nusselt number (continued).

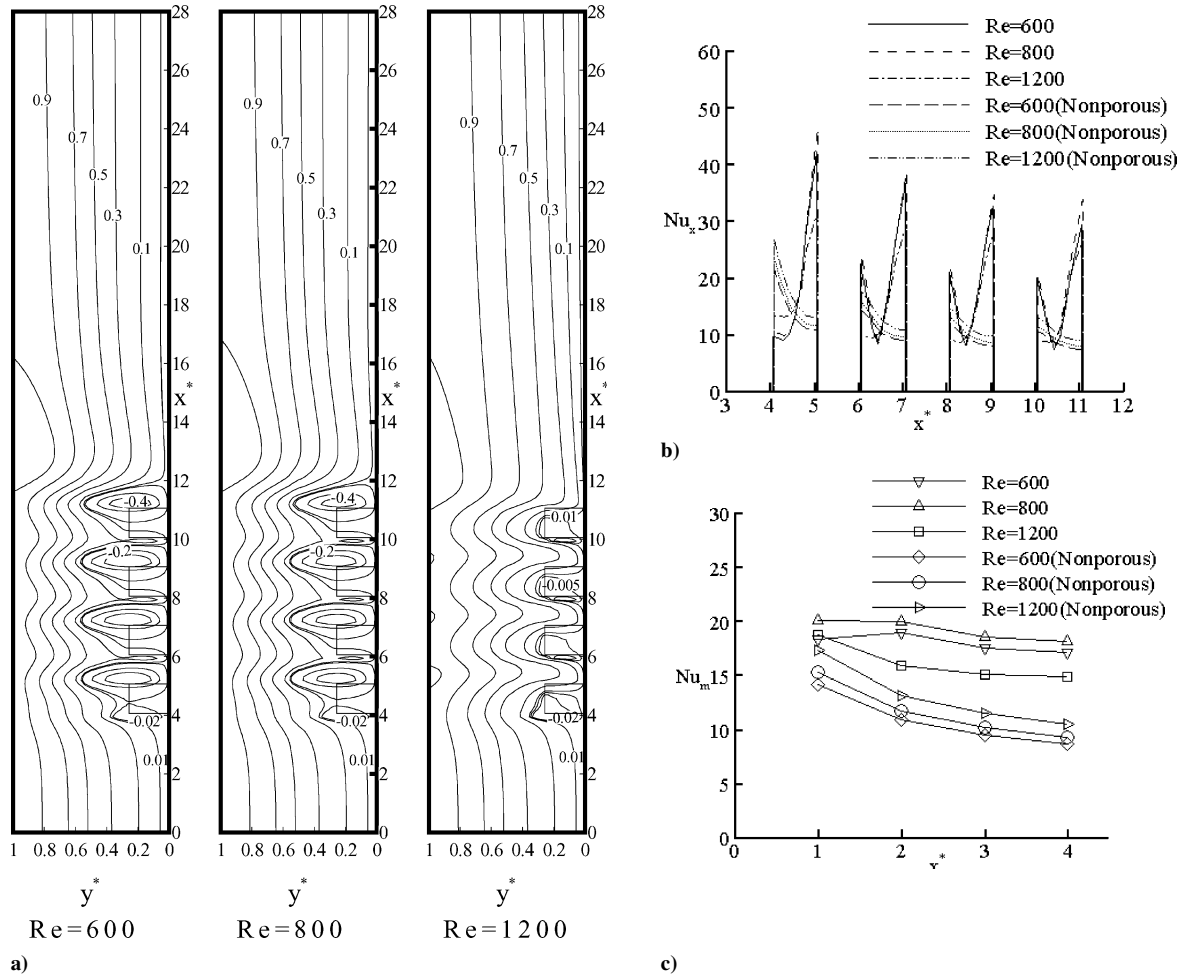

Fig. 6 Effects of the Reynolds number for $Da = 1 \times 10^{-5}$, $\Lambda = 0.35$, $Pr = 0.7$, $Gr_f = 3.6 \times 10^5$, $\lambda = 1$, $H^* = 0.25$, $W^* = 1.0$, $S^* = 1.0$, $L_i^* = 4$, and $L_o^* = 28$ on a) streamlines, b) local Nusselt number, and c) average Nusselt number.

where Eq. (17) was used for the fluid and Eq. (18) was used for the porous region. In addition, to accommodate the solution of the transport equations in both the fluid and porous regions, the effective viscosity of the fluid-saturated porous medium is set to be equal to the viscosity of fluid. It has been found that this approximation provides good agreement with experimental data.[16] In this study, the computational domain was chosen to be larger than the physical domain to eliminate the entrance and exit effects and to satisfy continuity at the exit. A systematic set of numerical experiments was performed to ensure that the use of a fully developed velocity profile for the outflow boundary condition has no detectable effect on the flow solution within the physical domain. The mathematical model and the numerical scheme were checked by comparing the results obtained from the present numerical results with other relevant limiting cases available in the literature. The relevant studies for our case correspond to the problems of 1) laminar mixed convection in a plain vertical parallel-plate channel with localized heat sources, that is, $H^* = 0$, no porous substrate; 2) forced convection in a porous channel with localized heat sources, that is, $H^* \to 1$ and $W^* \to L^*$, full porous channel; and 3) forced convection between parallel plates with finite rectangular heat blocks, that is, $Da \to 0$. The results for first case are within better than 1% agreement with the data reported by Tomimura and Fujii,[17] as shown in Fig. 2a. The results for second case are within less than 2% agreement with the data

reported by Hadim,[18] as shown in the Fig. 2b. The third validation was made by a comparison with the study of Davalath and Barazitoglu[19] for three heated rectangular blocks in a channel. Comparisons between dimensionless wall temperature distributions along the block exposed faces calculated in Ref. 19 and the current analysis show discrepancies of less than 1% as shown in Fig. 3. Further more, to ensure that the solution is grid independent, the predicted average Nusselt number is computed over each heat source mounted with porous block in a vertical plane channel from various grid arrangements for a case with $Da = 1 \times 10^{-5}$, $Re = 600$, $\Lambda = 0.35$, $Pr = 0.7$, $Gr_f = 3.6 \times 10^5$, $\lambda = 1$, $H^* = 0.25$, $W^* = 1$, and $S^* = 1$. Note that the differences in Nusselt number Nu_m on each heat source for 300×104, 375×84, 400×70, 415×104 grids are less than 1.8%. Accordingly, the 400×70 grid is considered to be suitable for the present study.

Results and Discussion

In this section, the effects of governing physical parameters, such as the Darcy number Da, inertial parameter Λ, Reynolds number Re, Grashof number Gr_f, porous-to-fluid thermal conductivity ratio λ, and two geometrical parameters H^* on the flowfield, temperature field, local Nusselt number distribution, and average Nusselt number were explored. The fixed input parameters for all cases in the simulations were $H^* = 0.25$, $W^* = 1.0$, $S^* = 1.0$, $L_i^* = 4$, and $Pr = 0.7$. (The cooling fluid in the study is air.) Because these basic dimensionless parameters are required to characterize the system, a comprehensive analysis of various combinations of these parameters was done. Note that, to illustrate the flow and temperature fields clearly, only the portion that concentrates on the porous/fluid region and its close vicinity are presented. However, at all times, the much larger domain was always used for numerical calculations and interpretation of the results. In addition, for brevity, the main features and characteristics of some of the results are discussed, but the corresponding figures are not presented. Figure 4 shows the effects of the porous-block structure on the fluid flow and thermal convection heat transfer for a typical case with $Da = 1 \times 10^{-5}$, $Re = 600$, $\Lambda = 0.35$, $Pr = 0.7$, $Gr_f = 3.6 \times 10^5$, $\lambda = 1$, and $L_o^* = 28$. Several interesting features are found in Fig. 4. The presence of the porous-block array causes the streamlines to bend significantly in the channel (Fig. 4a). The velocity distribution is parabolic at both the entrance and exit of the channel. However, this distribution changes rapidly as the fluid encounters the porous block array, especially at the corners of block. Another interesting feature is the formation of relatively large vortices behind each porous block separated by a small recirculation region rotating in a direction opposite to that of the larger vortices. The height of these recirculation regions is about twice that of the porous blocks. A weak eddy is generated on the smooth left plate, corresponding to the reattached region on the right plate. Here, the mechanism for the formation of these complicated flowfields within the channel is the consolidated result of five effects: 1) a penetrating effect pertaining to the porous medium, 2) a blowing effect caused by porous media displacing transversely the fluid from the porous region into the fluid region,[13,20] 3) a suction effect caused by the pressure drop behind the porous blocks resulting in a reattached flow, 4) the effects of boundary-layer separation, and 5) the buoyancy effect induced by

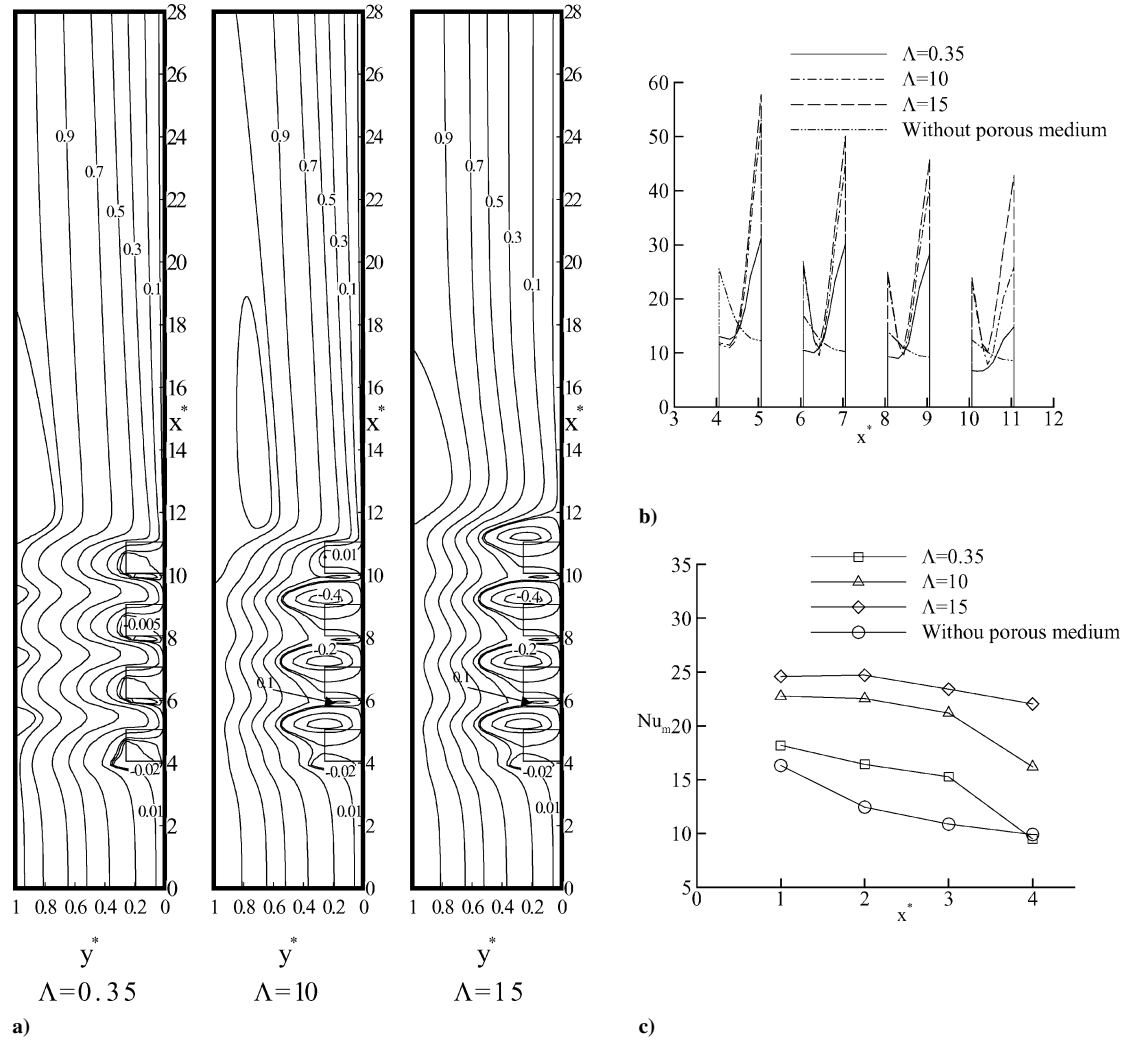

Fig. 7 Effects of the inertial number for $Da = 1 \times 10^{-5}$, $Re = 1000$, $Pr = 0.7$, $Gr_f = 3.6 \times 10^5$, $\lambda = 1$, $H^* = 0.25$, $W^* = 1.0$, $S^* = 1.0$, $L_i^* = 4$, and $L_o^* = 28$ with $\Lambda = 0.35$, 10, and 15 on a) streamlines, b) local Nusselt number distributions, and c) average Nusselt number.

finite heat sources. The interactions of the recirculations, caused by the porous blocks, with the core flow play a significant role in affecting the temperature field. The isotherm distribution corresponding to the described flowfield is shown in Fig. 4c. An interesting feature is that the thermal boundary-layer thickness increases over the porous blocks and decreases downstream from the porous blocks. This is different from a thermal boundary that develops from a flat finite heat source array placed along the right wall. In this problem, the distortion of isotherms arises partly due to the periodical cross-streamwise displacement of fluid from the porous region into the fluid region occurring at the porous-block array and intermittent transverse conduction in the fluid from the discrete heat sources. The variation of local Nusselt number corresponding to the described temperature field is shown in Fig. 4d. A periodic variation of Nusselt number Nu_x on the right plate is observed, with a decreasing mean. The local Nusselt number distribution is sharply peaked at leading and trailing edges of each heat source and drops steeply toward the heater middle part, where the larger and smaller vortices inside each heat source meet and a minimum Nusselt number Nu_x is reached. This can be explained by noting that there are two thermal boundary layers starting to develop from the leading and trailing edges of each heat source. Under the clockwise and counterclockwise recirculating actions caused by the porous matrix attached to the source surface, both thermal-boundary-layer thicknesses grow quickly along the source surface and join together at around the meeting location of the larger and smaller vortices (as shown in Fig. 4b). The heat transfer in the rear part of heat source is higher due to increased convection aided by higher velocities in the recirculation eddy. Although the heat transfer at around the location where the larger and smaller vortices meet is lower due to an almost stagnant flowfield within that region. In the heat source array, Nusselt numbers Nu_x or Nu_m decrease for downstream sources except source one. The reason is that as the fluid passes over the sources its temperature increases and the heat transfer coefficient decreases. The first source has smaller Nusselt number Nu_x value at the leading edge than the downstream sources due to the impact of the core flow as it penetrates the porous block array with a relative small vortex shedding at the front part of block 1 and lower temperature gradient at the leading edge of heat source 1. For the pure flat heat source array, a large Nusselt number occurs at the leading edge of each heat source where the intermittent thermal boundary layer begins to grow, and then Nusselt number declines toward the downstream edge due to boundary-layer growth. The Nusselt numbers in the insulated region separating the heat sources are zero. Similar results are found in the work of Tomimura and Fujii.[17] Comparison of average Nusselt number over each heat source with and without porous block shows that the recirculation flow caused by a porous block can augment significantly the heat transfer rate, as shown in Fig. 4e.

Effect of Darcy Number

The Darcy number $Da = K/R^2$ is directly related to the permeability of the porous medium. To investigate the effect of Darcy number on flow and temperature fields, computations were carried out at $Da = 1 \times 10^{-5}$, 2×10^{-5}, 1×10^{-4}, and 1×10^{-3} for $\Lambda = 0.35, Re = 600, Gr_f = 3.6 \times 10^5, \lambda = 1$, and $L_o^* = 28$. The flowfields shown in Fig. 5a reveal that for the range of Darcy number Da investigated the distortion of streamlines and the size of recirculations behind the porous blocks becomes less pronounced as Darcy number Da increases. This is due to the combined effect of the smaller bulk frictional resistance that the flow encounters at larger

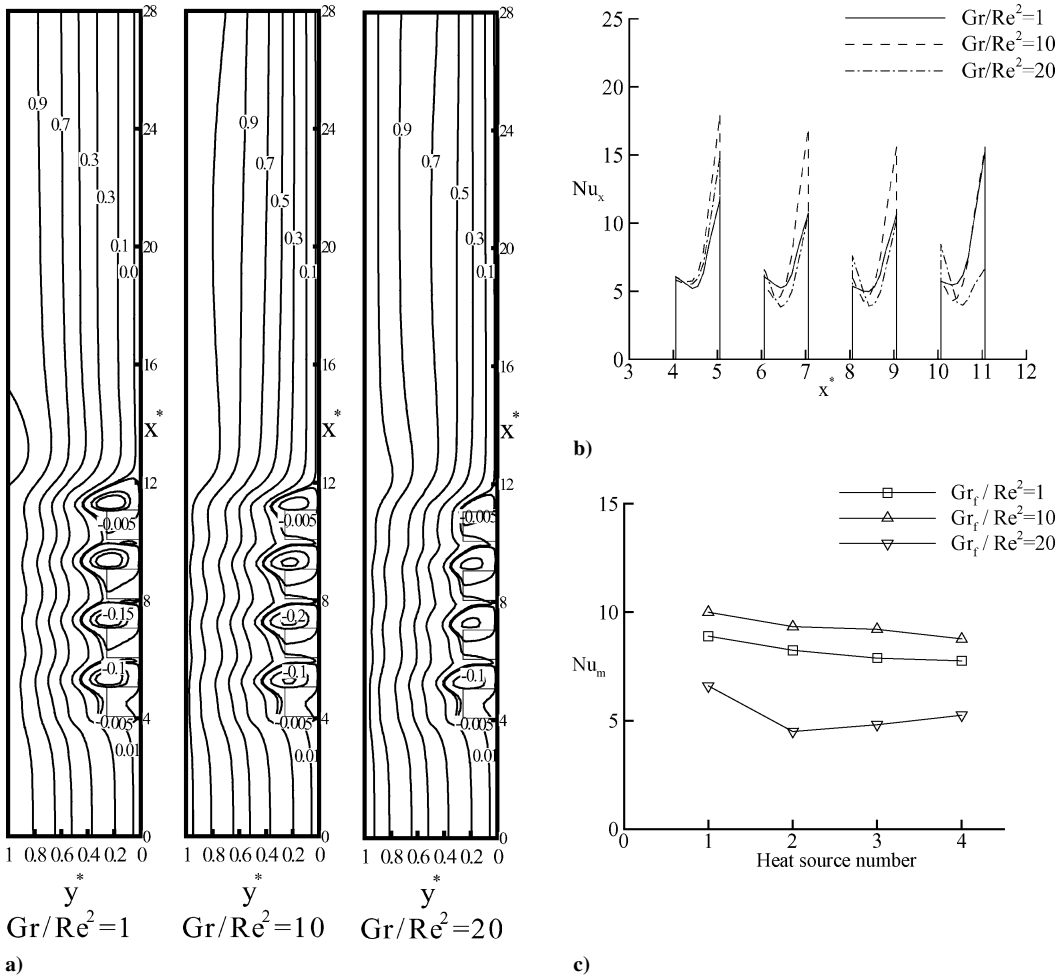

Fig. 8 Effects of the Grashof number for $Re = 600$, $Da = 5 \times 10^{-5}$, $\Lambda = 0.35$, $Pr = 0.7$, $\lambda = 1$, $H^* = 0.25$, $W^* = 1.0$, $S^* = 1.0$, $L_i^* = 4$, and $L_o^* = 105$ with $Gr_f/Re^2 = 1$, 10, and 20 on a) streamlines, b) local Nusselt number distributions, and c) average Nusselt number.

values of Darcy number *Da* and the increasing intensity of buoyancy in the porous region. This in turn causes a smaller blowing effect through porous blocks, which displaces the fluid less deep into the core flow and confines the development of recirculation zones in the transverse direction. When Darcy number *Da* is increased up to 1×10^{-3}, the flow penetrates completely into the porous block array, and no recirculation vortices are created in the channel. The temperature fields, shown in Fig. 5b corresponding to different Darcy numbers show that when the Reynolds number *Re* is small, the global temperature fields are strongly interrelated, encompassing the entire domain from the right to the left surface of the channel. However, as Darcy number *Da* increases, the extent of distortion for isotherms become less pronounced. This is the direct result of the discussed flowfield. The relationship between Nusselt number Nu_x and Darcy number *Da* is shown in Fig. 5c. It is seen that as Darcy number *Da* increases from 1×10^{-5} to 1×10^{-3}, the two-peak type curves of local Nusselt number distribution decay gradually and then transform to one-peak type, with which the peak value of Nusselt number Nu_x appears at the leading edge of the each heat source. In addition, the variation with Darcy number *Da* of Nusselt number Nu_m is shown in Fig. 5d. Here there is an interesting phenomenon for Nusselt number Nu_m over each heat source. In the calculation range of Darcy number *Da*, there exists a critical Darcy number corresponding to the smallest values of Nusselt number Nu_m over each heat source, beyond which the average heat transfer rate increases.

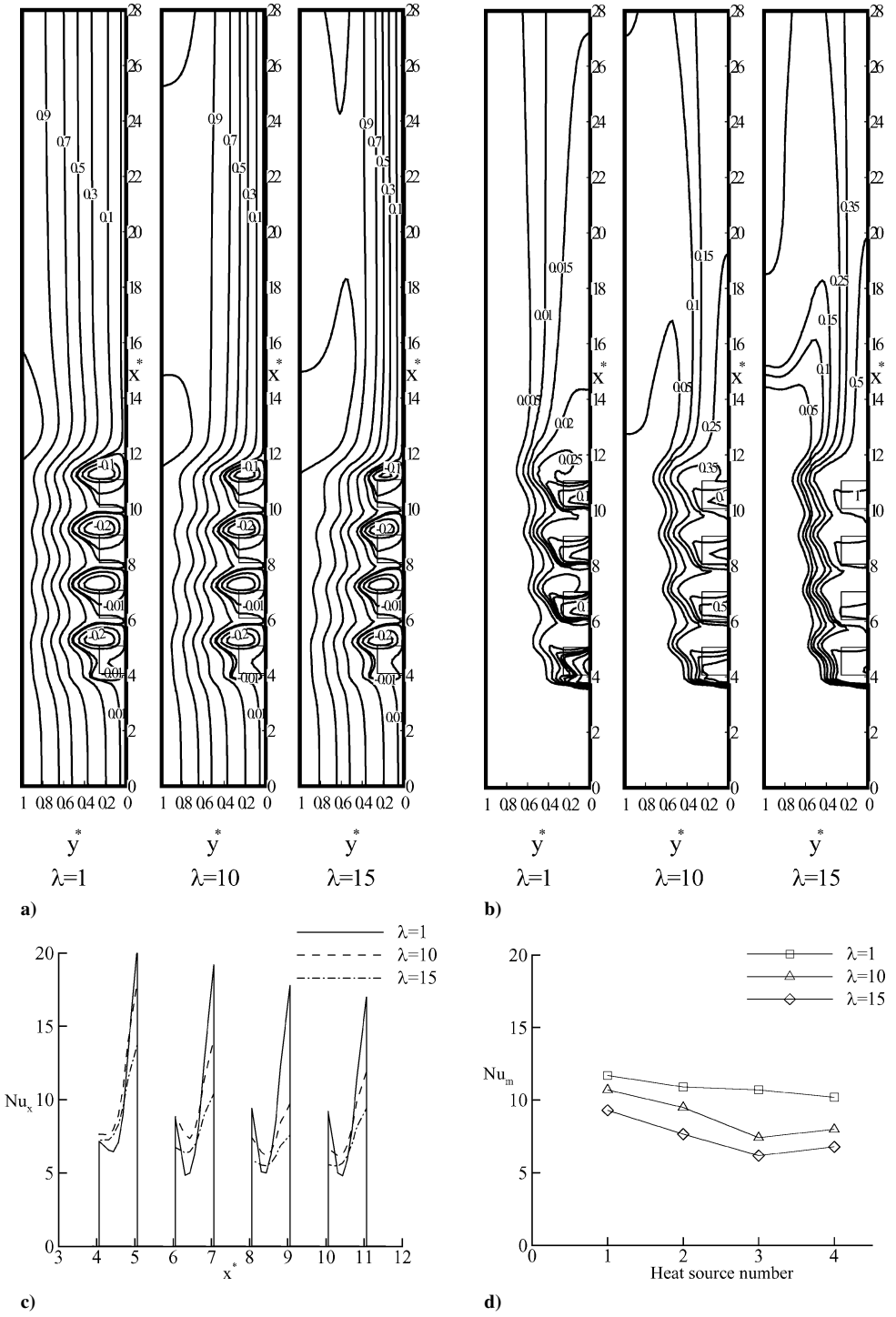

Fig. 9 Effects of variations in thermal conductivity ratio for the baseline case with λ = 1, 10, and 15 on a) streamlines, b) isotherms, c) local Nusselt number distributions, and d) average Nusselt number.

Effect of Reynolds Number

The effect of variations in the Reynolds number is shown in Fig. 6 for $Da = 1 \times 10^{-5}$, $\Lambda = 0.35$, $Pr = 0.7$, $Gr_f = 3.6 \times 10^5$, $\lambda = 1$, and $L_o^* = 28$ with $Re = 600$, 800, and 1200, respectively. The flowfields shown in Fig. 6a reveal that increasing Reynolds number *Re* from 600 to 800 slightly increases the distortion level in the core flow streamlines. The recirculation regions become slightly smaller and stronger. The reason for this trend is that increasing Reynolds number *Re* increases the fluid's forward momentum, resulting in a larger penetration into the porous matrix. This, in turn, reduces the action of the blowing effect caused by porous medium and restrains the expansion of recirculation flows in the transverse direction. As Reynolds number *Re* is increased further up to 1200, the larger vortex behind each porous block diminishes and ultimately vanishes. At the same time, the size of the smaller vortex ahead of each block grows, occupying most of the porous block. The effect of Reynolds number on the local and average Nusselt number is shown in Fig. 6b and 6c. Nusselt number Nu_x slightly increases with increasing Reynolds number *Re* from 600 to 800 because of the increased convection aided by higher velocities in the recirculation flow, whereas Nusselt number Nu_x decreases with increasing Reynolds number *Re* from 800 to 1200 due to the reducing convection caused by the weak and closed vortex inside the porous blocks, except source one.

Inertial Effects

The inertial parameter $\Lambda = FR\varepsilon/\sqrt{K}$ is concerned with microstructure of the porous solid matrix, which causes an increase in the inertial effects at higher velocity.[12] The effect of an increase or decrease in the inertial parameter Λ is shown in Fig. 7 for $Da = 1 \times 10^{-5}$, $Re = 1000$, $Pr = 0.7$, $Gr_f = 3.6 \times 10^5$, and $L_o^* = 28$ with $\Lambda = 0.35$, 10, and 15. Comparison of the streamlines in Fig. 7a reveals that the vortex behind each porous block gradually grows inside the interporous-block spacing as the inertial parameter increases. The reason for this is that the larger bulk frictional resistance caused by porous matrix decelerates the core flow, which leads to a larger blowing effect and creates a larger recirculation in the side top corner of porous blocks after encountering the primary flowfield. Figure 7b shows the variation of Nusselt number Nu_x with Λ. In general, as Λ increases, Nusselt number Nu_x increases. This is due to the larger fluid mixing caused by a larger recirculation zone for larger Λ. As expected, larger Λ results in higher Nusselt number Nu_m.

Effect of Grashof Number

Figure 8a shows the effects of buoyancy on the flow structure for $Da = 5 \times 10^{-5}$, $\Lambda = 0.35$, $Pr = 0.7$, $\lambda = 1$, $H^* = 0.25$, $W^* = 1.0$, $S^* = 1.0$, and $L_o^* = 105$. A series of calculations was carried out by varying the strength of the mixed convection, Gr_f/Re^2, in the range of 1–20, while the Reynolds number was fixed at $Re = 600$. The streamlines shown in Fig. 8a reveal that as the ratio Gr_f/Re^2 is raised, the size of larger recirculation behind each porous block, except the block 1, reduces and finally vanishes. Because of an increasing upward motion caused by buoyancy, the fluid penetrates deeper into the porous block, which reduces the blowing effect and limits the growth of the recirculation zone. The variation in local heat transfer rate Nusselt number Nu_x with Gr_f/Re^2 is in Fig. 8b. As seen in Fig. 8b, Nusselt number Nu_x in the front part of the

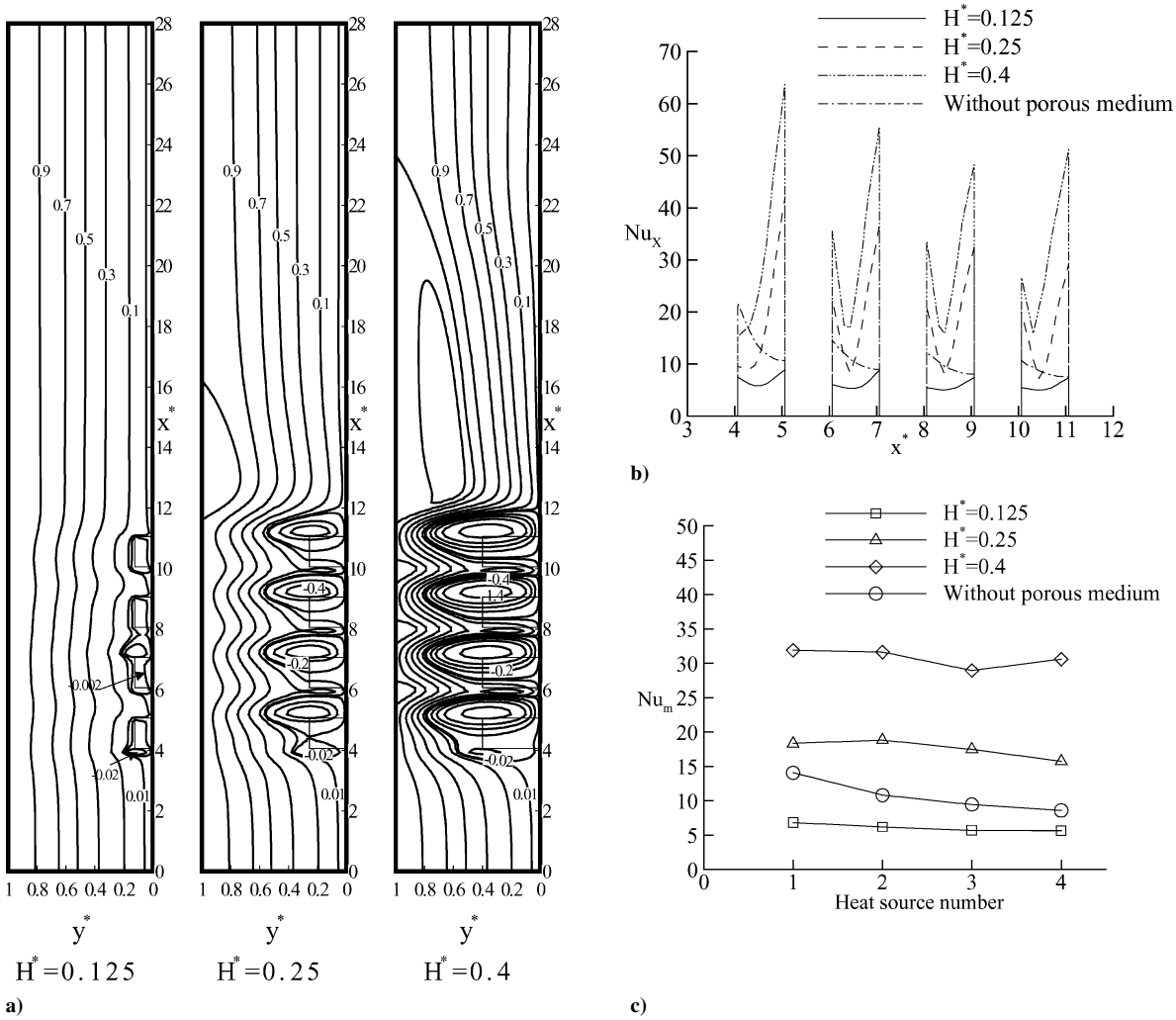

Fig. 10 Effects of the geometric parameters H^* for $Da = 1 \times 10^{-5}$, $\Lambda = 0.35$, $Re = 600$, $Gr_f = 3.6 \times 10^5$, $Pr = 0.7$, $\lambda = 1$, $W^* = 1.0$, $S^* = 1.0$, $L_i^* = 4$, and $L_o^* = 28$ on a) streamlines, b) local Nusselt number distributions, and c) average Nusselt number.

heat source increases, whereas it decreases in the rear part of the heat source as Gr/Re^2 increases from 1 to 20. For the first heat source, Nusselt number Nu_x decreases with increasing Gr_f/Re^2 because recirculation flow patterns are slightly sensitive to the variation in Gr/Re^2. As expected, Nusselt number Nu_m decreases with Gr_f/Re^2, as shown in Fig. 8c.

Effects of Conductivity Ratio

The effect of the thermal conductivity ratio is shown in Fig. 9 for fixed values of $Da = 1 \times 10^{-5}$, $\Lambda = 0.35$, $Re = 600$, $Pr = 0.7$, $Gr_f = 3.6 \times 10^5$, $H^* = 0.25$, $W^* = 1.0$, $S^* = 1.0$, and $L_o^* = 105$ with $\lambda = 1$, 10, and 15, respectively. Figure 9a shows that, as λ increases, the size and relative strength of recirculation zones around the porous blocks decrease. The reason for that is as λ is increased while Grashof number Gr_f and Darcy number Da are kept constant, the buoyancy effects decrease in the porous region (from the equation $Gr_{\text{eff}} = Gr_f \times Da/\lambda$), leading to confinement of the expansion of recirculation zone into the core flow. Figures 9b and 9c show that as the conductivity ratio increases there results a decay in the two-peak-type curve of local Nusselt number distributions and average Nusselt numbers over each heat source. This is because the increase in conduction heat transfer is less than the decrease in convection heat transfer.

Effect of Geometric Parameter H^*

Figure 10 shows the changes in flowfield and Nusselt numbers as the porous block height decreases H^* from 0.4 to 0.125 for $Da = 1 \times 10^{-5}$, $\Lambda = 0.35$, $Re = 600$, $Gr = 3.6 \times 10^5$, $Pr = 0.7$, $\lambda = 1$, $W^* = 1.0$, $S^* = 1.0$, and $L_o^* = 28$. As can be seen in Fig. 10a the distortions for the streamlines and isotherms become less pronounced as the block height decreases. In addition, the size of recirculation and the interaction between successive porous blocks reduce. This is due to the relative decrease in the height of the porous block, which in turn offers a lower degree of obstruction to the flow and a smaller blowing action for smaller values of H^*. Figures 10b and 10c show that Nusselt number Nu_x increases with increasing H^* due to the larger fluid mixing velocity and heat transfer area provided by the higher porous blocks.

Conclusions

A numerical study of laminar mixed convection of multiple heat sources mounted with porous blocks in a vertical parallel-plate channel was performed. The rectangular porous blocks change the incoming velocity field considerably, resulting in the formation of vortices penetrating these porous blocks. The strength and extent of these vortices, which strongly depend on five competing effects of penetrating, blowing, suction, boundary-layer separation and reattachment, and buoyancy, have profound influences on the heat transfer characteristics. The dependence of streamlines, isotherms, and local and average Nusselt numbers on the governing parameters is documented in detail. The computational results show that the increase in heat transfer rate is more pronounced at both trailing and leading edges of the strip heaters by altering some parametric values. Furthermore, the average heat transfer rate increases with the inertial parameter and dimensionless height of the porous block and decreases with Grashof number and the conductivity ratio. However, the effects of Reynolds and Darcy numbers are not straightforward. There exists a critical value for which the heat transfer rate is maximum (for Reynolds number) or minimum (for Darcy number). Below and above this critical value, the average Nusselt numbers of heaters drop off or go up.

Acknowledgment

The first author gratefully acknowledges the support of the National Science Council of the Republic of China through Contact NSC91-2212-E-027-010.

References

[1]Kim, S. J., and Lee, S. W., *Air Cooling Technology for Electronic Equipment*, CRC Press, New York, 1996, pp. 173–202.

[2]Nield, D. A., and Bejan, A., *The Convection in Porous Media*, Springer-Verlag, New York, 1992, pp. 321–343.

[3]Koh, J. C. Y., and Colony, R., "Heat Transfer of Microstructures for Integrated Circuits," *International of Communication of Heat and Mass Transfer*, Vol. 13, No. 1, 1986, pp. 89–97.

[4]Tien, C. L., and Kuo, S. M., *Cooling Technology for Electronic Equipment*, Hemisphere, New York, 1988, pp. 285–294.

[5]Kou, H. S., and Lu, K. T., "Combined Boundary and Inertia Effects for Fully Developed Mixed Convection in a Vertical Channel Embedded in Porous Media," *International Communications in Heat and Mass Transfer*, Vol. 20, No. 3, 1993, pp. 333–345.

[6]Hadim, A., "Numerical Study of Non-Darcy Mixed Convection in a Vertical Porous Channel," *Journal of Thermophysics and Heat Transfer*, Vol. 8, No. 2, 1994, pp. 371–373.

[7]Reda, D. C., "Mixed Convection in a Liquid-Saturated Porous Medium," *Journal of Heat Transfer*, Vol. 110, No. 1, 1988, pp. 147–154.

[8]Choi, C. Y., Lai, F. C., and Kulacki, F. A., "Mixed Convection in Vertical Porous Annuli," *AIChE Symposium Series 269*, Vol. 85, No. 269, 1989, pp. 356–361.

[9]Lai, F. C., Prasad, V., and Kulaki, F. A., "Aiding and Opposing Mixed Convection in a Vertical Porous Layer with a Finite Wall Heat Source," *International Journal of Heat and Mass Transfer*, Vol. 31, No. 5, 1988, pp. 1049–1061.

[10]Hadim, A., and Chen, G., "Non-Darcy Mixed Convection in a Vertical Porous Channel with Discrete Heat Sources at the Walls," *International Communications in Heat and Mass Transfer*, Vol. 21, No. 3, 1993, pp. 377–387.

[11]Hunt, M. L., and Tien, C. L., "Effects of Thermal Dispersion on Forced Convection in Fibrous Media," *International Journal of Heat and Mass Transfer*, Vol. 31, No. 2, 1988, pp. 301–310.

[12]Vafai, K., and Tien, C. L., "Boundary and Inertial Effects on Flow and Heat Transfer in Porous Media," *International Journal of Heat and Mass Transfer*, Vol. 24, No. 2, 1981, pp. 195–203.

[13]Huang, P. C., and Vafai, K., "Flow and Heat Transfer Control over an External Surface Using a Porous Block Array Arrangement," *International Journal of Heat Mass Transfer*, Vol. 36, No. 16, 1993, pp. 4019–4032.

[14]Adams, J., and Ortega, A. J., "A Multicolor SOR Method for Parallel Computation,"*Proceedings of the International Conference on Parallel Procession*, IEEE Computer Society Press, Piscataway, NJ, 1982, pp. 53–56.

[15]Patanker, S. V., *Numerical Heat Transfer and Fluid Flow*, Hemisphere, Washington, DC, 1980, pp. 79–138.

[16]Neale, G., and Nader, W., "Practical Significance of Brinkman's Extension of Darcy's Law Coupled Parallel Flows within a Channel and a Bounding Porous Medium," *Canadian Journal of Chemical Engineering*, Vol. 52, No. 4, 1974, pp. 475–478.

[17]Tomimura, T., and Fujii, M., "Laminar Mixed Convection between Parallel Plate with Localized Heat Sources," *Cooling Technology for Electronic Equipment*, edited by W. Aung, Hemisphere, Washington, DC, 1988, pp. 233–247.

[18]Hadim, A., "Forced Convection in a Porous Channel with Localized Heat Sources,"*Journal of Heat Transfer*, Vol. 116, No. 2, 1994, pp. 465–472.

[19]Davalath, J., and Bayazitoglu, Y., "Forced Convection Cooling across Rectangular Blocks," *Journal of Heat Transfer*, Vol. 109, No. 2, 1987, pp. 321–328.

[20]Vafai, K., and Kim, S. J., "Analysis of Surface Enhancement by a Porous Substrate, " *Journal of Heat Transfer*, Vol. 112, No. 3, 1990, pp. 700–705.